

INTERACTION OF LASER RADIATION WITH MATTER. LASER PLASMA https://doi.org/10.1070/QEL16557

Formation of a carbon nanofilm on oil-coated KU-1 glass annealed by KrF laser radiation

P.B. Sergeev, N.V. Morozov, A.N. Kirichenko

Abstract. **The annealing of an oil layer on the output face of a KU-1 glass substrate in air by a high-power 80 ns KrF laser pulse is studied. A polymer-like hydrocarbon film up to 40 nm thick is found to form at laser radiation fluences F above 2 J cm^{-2} on the glass surface. The upper limit of $F \approx 6$ J cm^{-2} is determined by the damage of the glass samples whose size is approximately equal to the laser spot diameter (1 cm).**

Keywords: *carbon nanofilms, KrF laser radiation, laser plasma, transformer oil.*

1. Introduction

The formation of diamond coatings from the gas phase has opened ways for various technological applications of this material [1–4], which possesses unique physicochemical characteristics. Unique properties were also revealed for other carbon (C) and hydrocarbon (C:H) films, due to which they are highly demanded for [2–7]. In this context, a problem of searching for maximally convenient, reliable, and efficient ways to form corresponding coatings on different materials has arisen. Currently, the solution of this problem is a prime line of research.

When using C and C:H films as antireflection or protective coatings in solar cells; as phosphors in UV, VUV, and X-ray detectors; as orienting layers in liquid crystals; and in many other cases, these films should be deposited on large areas (above 1 cm^2) on the surface of transparent optical materials (OMs) [2–7]. A promising way to form such coatings is to use the scheme implemented in [8, 9], where C:H nanofilms were synthesised by applying laser radiation to the interface between an aromatic liquid and a transparent insulator through the insulator.

In the aforementioned scheme, under conditions of weak absorption of laser radiation (LR) in the transparent substrate and strong absorption in the liquid, the laser pulse energy can be spent almost entirely to form a plasma near the substrate surface, onto which hydrocarbon radicals will be deposited from the plasma layer. Such is the logic of this way to form C:H films. In essence, this one of the versions of implementing the concept of film synthesis using laser plasma. Its availability was proven in [8, 9].

However, there are some nuances: during multipulse synthesis of a C:H film according to this scheme, the film eventually ceases to grow with an increase in the number of pulses because of the LR absorption occurring in it. The ablation damage of the substrate surface also enhances [9]. Thus, this scheme is efficient in the single-pulse regime or if the number of LR pulses is very small; i.e., when nanothin films are formed. Nevertheless, this version of film synthesis may be promising, taking into account the current sound interest in nanofilms. Hence, it is necessary and urgent to study the potential of this synthesis regime using various laser sources. It is noteworthy that the same scheme (but using a femtosecond IR laser and gas media at the boundary with glasses and crystals) was applied quite recently in [10].

When carbon films must be formed on large OM surface areas, one should apply lasers with high pulse energies. Laser processing of large areas using step-by-step surface scanning with low pulse energies and high pulse repetition frequencies is less efficient. This finding, made when fabricating liquid crystal displays using electric-discharge XeCl lasers, stimulated the development of technological lasers of this type with pulse energies of ~1 J [11, 12].

KrF* (λ = 248 nm), ArF* (193 nm), and XeCl* (308 nm) excimer lasers can efficiently generate pulses with energies of 10 J or higher under electron beam pumping [13, 14]. These systems can operate at repetition frequencies up to several Hertz [14], due to which they can be used in the above-considered technological scheme. Excimer electron-beam lasers (EBLs) are still laboratory products: they are rather large-size, expensive and radiation-hazardous facilities. For this reason, their technological potential has been scarcely studied. Therefore, promising applications should be sought for to justify their further development. The formation of nanofilms on OMs may be one of these applications.

The purpose of this work was to investigate the possibilities of growing carbon nanofilms of ~1 cm^2 in area on KU-1 glass using a KrF EBL, with LR applied to the glass–hydrocarbon liquid interface through the glass. The LR source (λ = 248 nm, pulse energy ~10 J, pulse duration 80 ns) was the electron-beam laser facility ELA [13]. It was previously used to study the surface annealing of silicon wafers and arsenic implantation into them on areas up to 2 cm^2 [15–19].

KU-1 quartz glass, which is an available and inexpensive material, has high strength characteristics, and is widely used to fabricate transfer optics for UV lasers, was chosen as an object of our experiments. Not the last factor determining our choice was the existence of well-studied induced-absorption spectra of KU-1 glass [20, 21], due to which the absorption of

P.B. Sergeev, N.V. Morozov P.N. Lebedev Physical Institute, Russian Academy of Sciences, Leninsky prosp. 53, 119991 Moscow, Russia; e-mail: psergeev@sci.lebedev.ru;
A.N. Kirichenko Technological Institute of Superhard and Novel Carbon Materials, ul. Tsentral'naya 7a, Troitsk, 108840 Moscow, Russia

Received 27 October 2017; revision received 11 December 2017
Kvantovaya Elektronika **48** (2) 136–144 (2018)
Translated by Yu.P. Sin'kov

the films formed on the glass surface could easily be separated from the substrate absorption. In these experiments (see [22] for their first results), real-time monitoring of the film characteristics was based on spectral measurements.

2. Experimental

The KrF laser radiation with a wavelength $\lambda = 248$ nm was generated in the electron-beam laser facility ELA [13]. Its laser chamber contained a gas mixture composed of F_2 (4 Torr) and Kr : Ar=1 : 10 at a pressure of 1.5 atm. At this pressure, the facility provides maximally uniform distribution of KrF LR energy density over the entire output window 5 cm in diameter [13]. The laser cavity was formed by a rear concave mirror with a radius of curvature of 20 m and reflectance of 97% at $\lambda = 248$ nm and a flat output mirror with a reflectance of 25%. The cavity transparency was optimal, due to which a pulse with an energy up to 8 J and a duration $\tau = 80$ ns could be generated. The pulse shape was close to rectangular, with a rising edge width of no more than 10 ns [13]. The LR divergence was 10^{-2} rad under these conditions.

The samples of the first set were made of KU-1 quartz glass; they had a diameter of 13 mm and a thickness of 3.2 mm and were of third-grade surface finish. The quartz samples from the second set, which had a diameter of 20 mm and a thickness of 6 mm, were of second-grade surface finish. Below, the samples from the first set are denoted by a numeral (sample working number), and the samples from the second set are denoted by letter 'M' and a numeral.

The hydrocarbon liquid contacting the quartz plate output surface was chosen to be transformer oil (TO). According to [23], all TOs are mineral oils of high purity and low viscosity. They are mixtures of polycyclic aromatic and naphthenic hydrocarbons with molecular masses $M \approx 230-330$. Unlike toluene and benzene, which were used in [8,9], TO is not toxic. Figure 1 shows the optical density (OD) spectra recorded for a TO-containing cell with a thickness $t = 1$ cm and for a KU-1 quartz substrate with an oil layer. These spectral measurements showed that the TO absorption coefficient ($\alpha = \mathrm{OD}/t$) does not exceed 0.1 cm^{-1} in the wavelength range from 600 to 1100 nm. At $\lambda = 400$ nm, the absorption coefficient $\alpha \approx 7$ cm^{-1}; it rapidly increases with decreasing λ. For the oil layer, the OD measured at $\lambda = 400$ nm made it possible to estimate its thickness as ~10 μm. This provided an estimate of TO absorption at $\lambda = 248$ nm: $\alpha(248\ \mathrm{nm}) > 10^4$ cm^{-1}. Such a large TO absorption coefficient at the laser wavelength allowed us to simplify the experimental scheme used in [8,9]: we ruled out the cell with liquid and restricted ourselves to an oil layer, which was annealed by KrF laser. This 'simplification' was a forced one, because in the experiments with an oil-containing cell the quartz windows were destroyed even at LR energy densities (below, fluence F) ~2 J cm^{-2}.

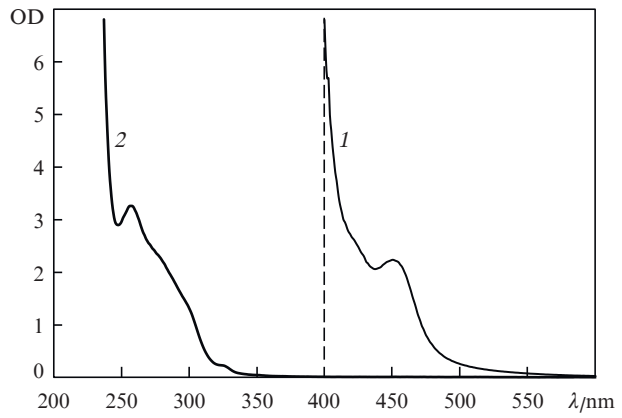

Figure 1. Dependences OD(λ) for (*1*) a 1-cm-thick TO-filled cell and (*2*) a quartz substrate with a TO layer ~10 μm thick. The layer thickness was estimated from the OD values at $\lambda = 400$ nm (vertical dashed line).

A schematic of the experiments on laser annealing of an oil layer on glass substrates was as follows. A laser beam (5 cm in diameter) from the ELA facility was focused by a planar-convex lens with a focal length of 40 cm. The radiation reflected from the output convex face of the lens was focused on a VChD-2 calorimeter [13], which measured the LR energy in each pulse. The laser beam cross section behind the lens focus in the region of the laser window image was 10 mm. That was the place of sample location. The fluence inhomogeneity in the irradiated spot did not exceed 10%. The second calorimeter (BKDM) was installed at a distance of 1 m from the lens [13]. Its readings in the absence of samples in the channel were used to calibrate the first calorimeter, which made it possible to determine the transmittance of the samples placed in the system. In these experiments, the maximum values of fluence F and intensity I_L reached 8 J cm^{-2} and 100 MW cm^{-2}, respectively.

A TO layer was deposited on the sample surface by a cotton-wool stick wetted in oil. Then a sample was installed vertically and kept in this position for ~5 min prior to irradiation in order to remove oil saggings from below. The OD spectrum of this film is shown in Fig. 1. Note again that the TO layer is located on the output (with respect to the laser beam propagation direction) side of the samples. This configuration prevents distortions of the specified fluence homogeneity in the region of LR interaction with TO and almost completely eliminates the radiation loss. Even with allowance for the short-lived LR absorption at $\lambda = 248$ nm in KU-1 glass, induced by plasma VUV light, this loss does not exceed 5%, as can be estimated based on the results of [24,25].

Optical methods are often used to monitor the properties of carbon nanofilms [6,26]. Using available Hitachi U-3900 and Genesys-2 spectrophotometers, we measured the transmittance of quartz samples to determine in real time the consequences of TO laser annealing. The spectral measurement ranges for Hitachi U-3900 and Genesys-2 are, respectively, 190–800 and 200–1100 nm. These instruments were also characterised by different cross sections of probe light beams on the sample surface: 5 × 5 mm for Hitachi U-3900 and 5 × 10 mm for Genesys-2. The transmission spectra of the samples were recorded by both spectrophotometers in the digital format with a step of 1 nm before (T_0) and after [$T(\lambda)$] laser irradiation. Then these data were used to plot the spectrum of the optical density induced in the corresponding process: $\mathrm{OD} = \ln(T_0/T)$. The OD spectra presented in Fig. 1 were obtained in the same way with the only distinction: here, T_0 and T are the transmittances of a cell or substrate without and with oil, respectively.

The surface structure of almost all samples was studied in an optical microscope with a magnification up to 160× before and after the KrF laser annealing of the oil layer. The surfaces of some samples were also investigated by Raman scattering (excitation with a 532-nm laser) using an inVia Raman Microscope Renishaw spectrophotometer (the United Kingdom).

3. Results on carbon films and discussion

In the experiments on TO annealing by KrF laser radiation, we varied the LR fluence and the number of laser pulses incident on the sample surface with a newly deposited oil layer. The number of the so-called cleaning laser pulses, irradiating the quartz plates after annealing the TO layer on them, was also varied. To establish the role of all these parameters in the process under study, it was necessary to irradiate and investigate more than 100 glass substrates in different regimes using the aforementioned equipment.

Figure 2 shows the OD spectra of a number of quartz samples and one sapphire substrate after annealing a TO layer on them by single KrF laser pulses with different fluences. These spectra can be divided into three types. The first-type spectra are observed at low fluences F, when the OD value does not exceed 0.04 even near the short-wavelength edge (~200 nm). An example is the spectra of samples M13 and M18 in Fig. 2. The upper limit of F for the samples exhibiting these spectra (F_m) is close to 2 J cm^{-2}. No changes in the structure of the irradiated surface of these samples can be observed in an optical microscope. Apparently, under these TO annealing conditions, the oil layer is partially evaporated under laser irradiation and moved off by a formed vapour layer.

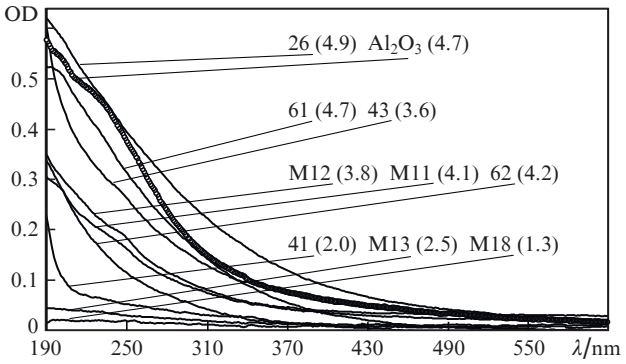

Figure 2. Dependences OD(λ) for C:H films formed on different samples. The values in parentheses after the sample number are KrF LR fluences (in J cm^{-2}) at which TO layers were annealed.

The second-type spectra are characterised by a sharp absorption peak in the range of 190–200 nm, as for sample 41 (2.0) in Fig. 2. These spectra were recorded for the plates with a TO layer annealed at LR fluences exceeding F_m by 1 J or less. For these samples, as well as for all other samples processed with $F > F_m$, surface melting traces were observed in a microscope. Therefore, the value $F_m \approx 2$ J cm^{-2} can be considered as a surface melting threshold for KU-1 samples coated by a TO layer annealed by a KrF laser pulse with $\tau = 80$ ns.

The behaviour of the second-type OD spectra is described well by a function proportional to λ^{-4}. This fact indicates that the losses are due to the scattering of short-wavelength radiation from the growing small inhomogeneities on the irradiated surface. It is likely that similar processes of surface melting occur on quartz plates with an oil layer and on silicon plates under irradiation of a surface area of ~1 cm^2 by a KrF laser. Rare melt nucleation points with a characteristic 'frozen' ring structure near these points arose first on the silicon surface after the exposure to LR pulses [18, 19]. The number of these points and the area of the ring structures around them increased with an increase in F. Then the surface waves from different points overlapped, and one could observe melting of the entire surface, which acquired a wavy structure [18, 19]. Therefore, in the case of large laser spot cross sections on the irradiated sample surface, it is expedient to introduce the concepts of the 'melting threshold of the entire surface' (F_s) and the 'melting range' ($\Delta F = F_s - F_m$). They characterise more precisely the melting of large surfaces, which starts and develops on their different defects. When annealing an oil layer on quartz samples by a KrF laser, $\Delta F \approx 1$ J cm^{-2} at $F_s \approx 3$ J cm^{-2}.

Finally, the third-type spectra in Fig. 2 are characterised by absorption that smoothly but rapidly increases with a decrease in wavelength from ~500 to 190 nm, as for the samples exposed to fluences above 3 J cm^{-2}. This absorption is due to the formation of a hydrocarbon C:H film on the glass surface [22]. The contributions from the quartz substrate and residual oil traces to these spectra will be considered below.

The samples characterised by the third-type spectra (Fig. 2) exhibited a rise in absorption with an increase in the LR fluence. To refine this observation, the results for all samples on which TO films were annealed by a single KrF laser pulse are compiled in Fig. 3 in the form of dependences of OD(250 nm) on F. The results for the samples characterised by the first- and second-type absorption spectra [for which OD(250 nm) $\leqslant$ 0.03] were rejected. The solid line in Fig. 3 is a linear approximation for the entire set of points. It indicates the existence of a threshold fluence value, after which OD(250 nm) starts rising; this value corresponds approximately to the midpoint of the melting range. This line, as will be shown below, is a manifestation of the rise in the thickness of C:H films with an increase in F.

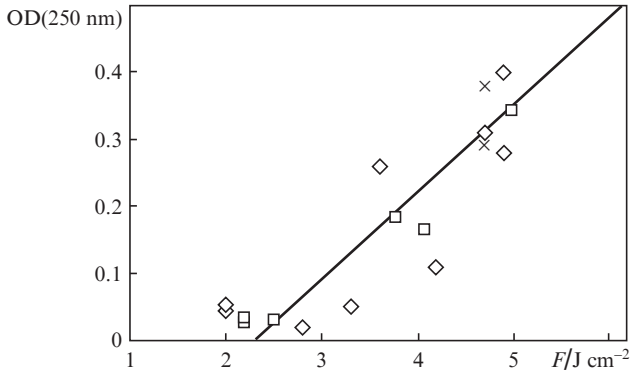

Figure 3. Experimental OD(250 nm) values for C:H films formed as a result of annealing of TO layers on quartz samples from the (□) first and (◇) second sets and (×) on sapphire plates by one laser pulse with a corresponding fluence F. The solid line is a linear approximation for all experimental points.

Figure 4 shows the data on the multipulse effect of LR on the TO films newly deposited on sample after each pulse [22]. Samples 26–28 were exposed, respectively, to one pulse with $F = 4.9$ J cm^{-2}, two pulses with $F \approx 4.3$ J cm^{-2}, and four pulses with $F \approx 3.5$ J cm^{-2}. Sample 30 was exposed to ten pulses with an average fluence of $F = 3.5$ J cm^{-2}. It can be seen in Fig. 4 that an increase in the number of pulses affecting the oil film leads to a decrease in the OD throughout the entire spectrum. This fact indicates that the thickness of primary films on the glass (obtained after TO annealing) decreases with increasing number of laser pulses. Based on the rate of the decrease in

the film thickness from sample to sample with a rise in the number of pulses, one can say that the film thickness tends to a constant value, in correspondence with the results of [9].

The thin curves in Fig. 4 show the results obtained with the Genesys-2 spectrophotometer for the same samples. It can be seen that for the OD value for sample 26 obtained in these measurements is smaller by a factor of about 1.4 than that determined using Hitachi U-3900. The spectra for sample 27 almost coincide. The optical densities of samples 28 and 30, measured on Genesys-2, are about 20% larger (they are omitted in Fig. 4). Since the probe light beams have different cross sections in these instruments, the differences in the OD values for identical samples, revealed with their aid, are due to the inhomogeneities of C film thickness. These inhomogeneities determine the error in measuring OD, equal to ~20%. Note that the maximum thickness homogeneity for the primary films on quartz samples is obtained when annealing TO layers by two KrF laser pulses.

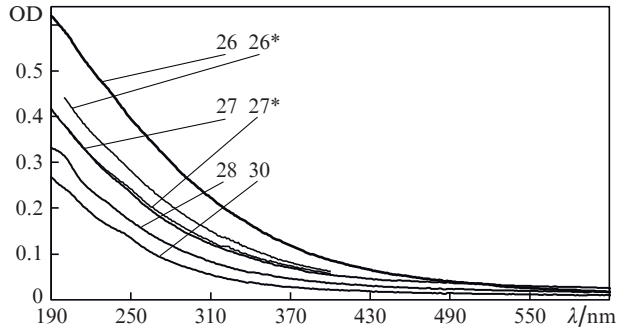

Figure 4. Dependences OD(λ) for C:H films formed on different samples. The spectra recorded with Hitachi U-3900 and Genesys-2 spectrophotometers are indicated, respectively, by numerals (sample numbers) and numerals with asterisk.

The first test of the physical properties of the films was their 1-h heating in air in a Petri dish at a temperature of 480°C. The difference in the optical densities of the samples in the range $\lambda > 400$ nm before and after heating (ΔOD) was ± 0.02, a value close to the determination error. An increase in ΔOD to 0.04–0.06 was observed in the region of $\lambda \approx 200$ nm. The structure of the difference spectra demonstrates that the ΔOD value is sometimes related to the annealing of the induced absorption in the glass (annealing of E centres and nonbridging oxygen atoms [20,21]) or to the annealing of the residual oil layer ~10 nm thick. Therefore, the value $\Delta OD \approx 0.05$ can be considered as a methodical error in determining OD in the region of $\lambda = 200$ nm for the nanofilms formed on glass. With allowance for these remarks, we find that the 1-h heating of quartz samples with primary films at a temperature of ~500°C barely affects their optical characteristics. This thermal durability in air is a characteristic feature of C and C:H films [2–6].

Laser cleaning of quartz samples after annealing the TO films formed on them revealed some other properties of these films. The samples whose OD spectra are presented in Figs 2 and 4 have a transmittance higher than 60% at $\lambda = 250$ nm and OD(250 nm) < 0.4. However, for the first cleaning KrF laser pulse at $F > 1$ J cm^{-2}, the integral (during the pulse) LR transmittance of the samples characterised by third-type OD spectra was found to be less than 10%, which corresponds to OD(250 nm) > 2.2! This fact is indicative of strong nonlinear absorption of KrF laser radiation in this process even at intensities I_L ~10 MW cm^{-2} or higher. The nature of this effect is unknown.

Subsequent cleaning pulses lead to an increase in the LR transmittance of the samples to the pure-substrate level (under the fourth or fifth pulse). The rate of the change in the film characteristics in the cleaning stage depended also on the number of preceding pulses and the LR fluence. These dependences are multiparameter ones. Therefore, it is expedient to suspend their study (which calls for long time) until specific practical problems arise. Especially as there is some experience in the modification of C:H films by direct multipulse irradiation using a KrF laser [2, 27, 28].

The third-type OD(λ) spectra presented in Figs 2 and 4 in the entire measurement range (from 190 to 1000 nm) are best described as follows:

$$\mathrm{OD}(\lambda) = \mathrm{OD}_0 \exp[B(\lambda_0 - \lambda)]. \quad (1)$$

Here, OD_0 is the OD value at the wavelength $\lambda_0 = 250$ nm. The coefficients B for different spectra varied in the range of 0.012 ± 0.002 nm^{-1}. Note that the OD(λ) spectrum of sample 30 at $B = 0.012$ nm^{-1} almost coincided with the spectrum of a C film deposited on a quartz sample under KrF laser irradiation of a graphite plate instead of TO. At the same coefficient B, formula (1) described well the spectra of films deposited on two sapphire substrates; one of them is shown in Fig. 2. This proximity of the absorption spectra of different samples suggests identity of the optical transitions in the UV spectral region, which determine mainly the absorption in the films synthesised.

OD spectra allow one to estimate the thicknesses of the corresponding films if their absorption coefficients are known. According to the data reported in [2, 5, 6, 26] and in the studies cited therein, the absorption coefficient (α) of various carbon and hydrocarbon films at $\lambda = 250$ nm varies from $\sim 5 \times 10^4$ to $\sim 2 \times 10^5$ cm^{-1}. Accurate to 2, one can assume this coefficient to be 10^5 cm^{-1}. Then, using the OD(250 nm) data on the samples presented in Figs 2 and 4, we find that the thickness of the corresponding films does not exceed 40 nm (sample 26). Upon multipulse annealing of oil layers, proceeding from the data of Fig. 4, the thickness of the nanofilms formed on glass is stabilised at a level of ~10 nm (sample 30).

On the assumption that $\alpha(250\ \mathrm{nm}) = 10^5$ cm^{-1} for the synthesised nanofilms, we can estimate their another parameter: the width of the so-called optical gap E_{04}, which is determined from the energy of probe light photons at which the film absorption coefficient is 10^4 cm^{-1} [6, 26]. To this end, the experimental OD(λ) spectra are converted into OD(E) spectra, where $E = ch/\lambda$ is the energy of a light photon with a wavelength λ, c is the speed of light, and h is Planck's constant. Then $\alpha(E)$ spectra (in cm^{-1}) are constructed using the formula

$$\alpha(E) = 10^5 \mathrm{OD}(E)/\mathrm{OD}(5\ \mathrm{eV}), \quad (2)$$

where it is taken into account that the photon energy at $\lambda = 250$ nm is 5 eV. Figure 5 shows the thus obtained absorption spectra for 15 different samples with films and an averaged dependence, constructed using expression (1). It demonstrates how accurately formula (1) describes the real OD spectra at different E and λ values.

It can be seen in Fig. 5 that the E_{04} value for the majority of $\alpha(E)$ spectra lies in the range of 2.5–3 eV. Only for two samples (27 and 28) it is close to 2 eV. The mean E_{04} value ($\langle E_{04}\rangle$), averaged over all samples exposed to LR in different regimes, is 2.7 eV. For the samples on which TO was annealed by one LR pulse, $\langle E_{04}\rangle$ = 2.8 eV. Note that an increase or decrease in α(250 nm) = 10^5 cm^{-1} by a factor of 2 leads, respectively, to a decrease in $\langle E_{04}\rangle$ by 0.3 eV or an increase in $\langle E_{04}\rangle$ by 0.4 eV. This circumstance indicates that the error in determining E_{04} for nanofilms using the above-described technique does not exceed 15%. The importance of the E_{04} value is that it yields information about other nanofilm characteristics, in particular, the hydrogen content [6, 26, 29–31].

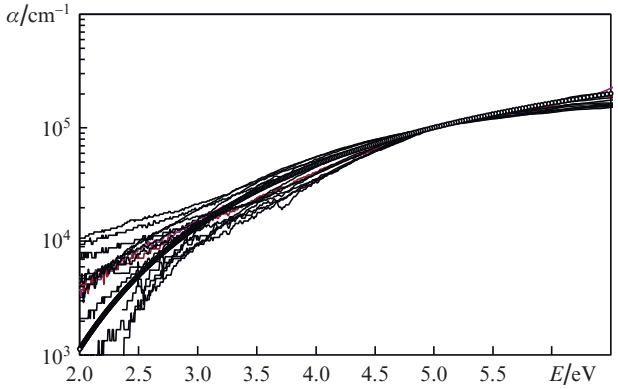

Figure 5. Dependences of the absorption coefficient of C:H films formed on different samples on the probe-light photon energy E, under the assumption that α(5 eV) = 10^5 cm^{-1} for all these films. The thick line is the averaged dependence, plotted based on formula (1).

An investigation of synthesised nanofilms on a Raman spectrophotometer made it possible to refine their composition. Here, we used the results of many original studies and reviews, e.g., [6, 29–31], in which both the physical fundamentals and the experience in application of Raman spectrophotometers for studying various C and C:H nanofilms were reported. These studies allow us not to go into details of Raman spectroscopy of carbon nanofilms and pass directly to the presentation of essential results obtained by this method.

Figure 6 shows some typical Raman spectra of quartz samples with nanofilms. The Raman spectra of samples 26, 27, 28, and 30 are similar. The signal intensity in these structureless spectra rises almost linearly with an increase in the Raman shift (ΔE). A specific feature of these spectra is the absence of a signal from the quartz substrate. A similar spectrum was observed for the film deposited on a sapphire substrate, although it exhibited lines at 650 and 750 cm^{-1} (characteristic of the Al_2O_3 crystal). The strong fluorescence signal, which obscures the characteristic Raman signal when the probe LR is in the visible range, is a distinctive spectral feature of polymer-like hydrocarbon films (PLCH, according to the classification of [6, 29–31]).

The Raman spectra of some other samples with nanofilms synthesised practically at the same fluences F as the films on samples 26 and 28, exhibited also bands from the quartz substrate (structures in the range ΔE < 1300 cm^{-1} [32]) and characteristic carbon bands, peaking at 1580 and 1340 cm^{-1} (G and D bands, respectively). The relationship between the intensities and half-widths of the D and G bands and the characteristics of carbon nanofilms was described in detail in [6, 29–31]. In Fig. 6, one can see D and G bands of different intensities in the five lower spectra.

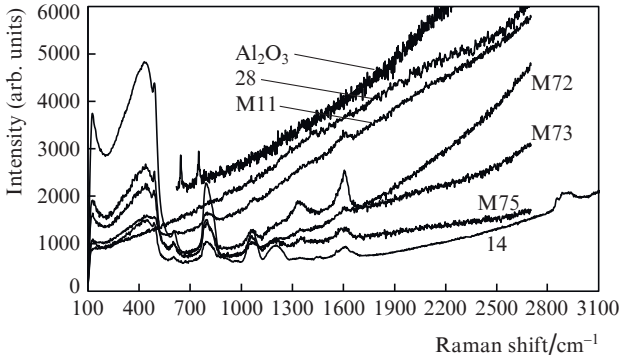

Figure 6. Raman spectra of different samples with films.

The nanofilm on sample M11 was formed as a result of exposure to one LR pulse with F = 4.1 J cm^{-2}. As can be seen in Figs 2 and 4, its OD(250 nm) almost coincides with that for sample 28; hence, the films formed on these samples have close thicknesses. However, the Raman spectra of the aforementioned samples differ: there is a pronounced G band peaking at 1600 cm^{-1} in the spectrum of M11. This difference can be due to variations in the hydrogen content ([H]) in C:H films: structureless Raman spectra are observed for PLCH films with [H] > 45% (percentage of the number of all atoms), while G bands manifest themselves for films with [H] ⩽ 45% [30, 31]. It was also noted in those studies that the slope m of the luminescence background in the Raman spectra of C:H films in the range $\Delta E \approx$ 1000–1800 cm^{-1} ($m = \Delta I/\Delta(\Delta E)$, where I is the Raman intensity) is related to [H]. It can be seen in Fig. 6 that the slopes of the Al_2O_3 spectra are practically the same for samples 28 and M11. Therefore, the hydrogen concentrations in the hydrocarbon films formed on these samples approximately coincide and correspond to the G-band occurrence threshold; i.e., they are about 45%.

The results of [30, 31] allow one to estimate the H content in films proceeding from the E_{04} value. For the group of samples subjected to single-pulse TO annealing, this estimation yields a value of 35% for the main version [α(250 nm) = 10^5 cm^{-1}] and 40% if α(250 nm) is half as small. It can be seen that the latter result (40%) makes it possible to match the [H] values obtained by different methods, under the assumption that their determination error is ±5%. Thus, almost all C:H nanofilms synthesised on quartz samples in the regime of single-pulse TO annealing have [H] ≈ 40% ± 5%. According to [6, 29–31], these nanofilms belong to polymer-like ones.

The nanofilm on sample M73 was formed after exposure to two KrF laser pulses with fluences of 4.7 and 4.3 J cm^{-2}. Its thickness is 12 nm. The Raman spectrum of this film (Fig. 6) contains a pronounced contribution from the quartz substrate and carbon D and G bands peaking at 1330 and 1600 cm^{-1}, respectively. Proceeding from the value m/I(G) = 7 μm, where I(G) is the peak intensity of the G band, one can estimate the [H] value as 36% [31]. An estimation based on the parameter E_{04} = 2.95 eV yields almost the same [H] content: 38%.

The C:H film on sample 27 was also obtained after two-pulse TO layer annealing at almost the same fluences as in the

case of sample M73. However, its thickness is 23 nm, which is almost twice as large as that of the M73 film. In addition, as was noted above, the Raman spectra of samples 27 and 28 are similar; hence, the hydrogen content in them is at a level of 45%. At the same time, an estimation of [H] based on E_{04} = 2–2.5 eV for sample 27 yields only 25–30%. What is the reason for this distinction?

An analysis of the experimental conditions showed that the difference in the parameters of the C:H films formed on samples 27 and M73 is caused by the difference in the thicknesses of the oil layers annealed on them. In the first stage, where the samples with numbers from 1 to 30 inclusively were irradiated, each TO layer was deposited as described above. In the later stages, different ways of depositing oil layers with thicknesses below conventional (10 μm) were tested. For example, the TO layer on sample M73 was formed before the second LR pulse by spreading a small amount of oil, remaining on the unirradiated sample surface after the first pulse, over the surface using a dry cotton-wool stick. This layer was much thinner than the second layer for sample 27. Similar differences were revealed for other pairs of samples with different films, obtained in similar laser irradiation modes. Hence, a necessary condition for the stability of the parameters of C:H nanofilms synthesised according to the above-considered technique is the stability of the laser parameters and the thickness of annealed TO layers.

The significant discrepancy in the contents [H] for the C:H film formed on sample 27, which were found proceeding from the Raman spectrum and the E_{04} value, may be related to the film thickness inhomogeneity and possible presence of oil traces on the surface. The presence of TO traces on the sample surface in the form of a film ~10 nm thick was observed in the experiments on their thermal annealing. This thin oil coating may distort significantly the Raman spectrum of a C:H film due to the rise in the luminescence background. In the OD spectra, as was mentioned above, the background contribution was up to 0.06 only at $\lambda < 230$ nm. In the range $\lambda > 250$ nm, where the E_{04} value is determined, such thin oil layers do not affect the nanofilm absorption.

It is reasonable to anneal possible oil traces on synthesised nanofilms by cleaning LR pulses. This procedure is convenient to implement using the main way of radiation supply: through the substrate. An analysis of the consequences of this irradiation showed that the E_{04} value for the primary nanofilms (synthesised using one LR pulse) reduced on average by 0.2 eV after exposure to a cleaning pulse with a fluence of ~1 J cm^{-2}. This reduction indicates a decrease in [H] in the films by about 2% [30,31], as confirmed by an analysis of Raman spectra. The OD(250 nm) of the samples changed randomly within the measurement error, a fact indicative of small variations in the thickness of C:H nanofilms.

Note another important nuance, which was revealed when analysing the laser cleaning of samples. The C:H film on sample M72, whose Raman spectrum is shown in Fig. 6, was formed as a result of irradiation by two LR pulses with F = 4.2 and 4 J cm^{-2} and subsequent exposure to one cleaning pulse with F = 4 J cm^{-2}. The film thickness is 9 nm, and E_{04} = 2.8 eV, which corresponds to [H] = 35%. This value is somewhat smaller than that for sample M73, which was not cleaned. Thus, we have another confirmation of the decrease in [H] after laser cleaning of films. However, a contradiction arises again. The Raman spectra of samples M72 and M73 exhibit a pronounced distinction: the M72 spectrum is characterised by a much steeper luminescence background. According to [30,31], this feature suggests a higher [H] content specifically for sample M72. Where does this contradiction come from?

A comparison of the OD spectra of these two samples showed the presence of strong absorption bands in the M72 spectrum, which are characteristic of the main defects in quartz glass (non-bridging oxygen atoms and E centres). May they be the reason? Indeed, Raman spectroscopy of KU-1 samples with a high content of main defects, induced by electron-beam irradiation [33], revealed a nonlinearly rising luminescence background in the range $\Delta E > 1000$ cm^{-1}, as for sample M72. Apparently, the first cleaning pulse with a large F (~4 J cm^{-2}) induces many intrinsic defects in the quartz substrate. In this case, the slope m of the luminescence background in Raman spectra cannot be used to estimate the [H] value for C:H films formed on quartz glass substrates [30,31].

The consequences of multipulse laser cleaning are demonstrated by the Raman spectrum of sample 14 in Fig. 6. A 9-nm-thick C:H film was formed on this sample after irradiation of newly deposited TO layers by three LR pulses with $F \approx 3$ J cm^{-2} and subsequent exposure to three more cleaning pulses with $F \approx 4$ J cm^{-2}. Here, the standard Raman spectrum of KU-1 glass dominates in the range $\Delta E < 1300$ cm^{-1}. A nonlinear background manifests itself at larger ΔE values; however, it is weaker than for sample M72, which is apparently related to the annealing of main glass defects [20,21,34] by the second and third cleaning laser pulses. The presence of a C:H film on sample 14 is evidenced in the Raman spectrum by the carbon G band at 1600 cm^{-1}, weak traces of the D band near 1350 cm^{-1}, and a band in the vicinity of 2900 cm^{-1}. For this film, E_{04} = 2 eV. Hence, according to [30,31], we find that [H] ≈ 25% for this film; however, this value is close to the applicability threshold of the method for estimating [H].

The nanofilm on sample M75, whose Raman spectrum is also shown in Fig. 6, was formed by laser irradiation of a graphite plate (instead of TO); it does not contain any hydrogen. Its thickness is 10 nm, and E_{04} = 2 eV, as well as for sample 14. Proceeding from the latter parameter, the hydrogen content is the same in these films. This comparison shows the accuracy of estimating [H] values for C:H nanofilms on quartz glass according to the technique proposed in [30,31] for [H] ≈ 25%. Taking into account these remarks, we find that, with the aid of cleaning LR pulses, the [H] value in synthesised C:H nanofilms can be reduced from the initial value of ~40% to less than 25%.

Note some more features in the Raman spectra of synthesised C:H nanofilms. For all the samples whose spectra exhibited carbon G bands, as in the five lower spectra in Fig. 6, the peaks of these bands were in a narrow range of 1600 ± 4 cm^{-1}. Their FWHMs also lied in a fairly narrow range: 75 ± 15 cm^{-1}. The peaks of the observed D bands were in range of 1340 ± 10 cm^{-1}, and their widths varied within 50–90 cm^{-1}. The intensity ratios in the peaks of D and G bands were in the range of ~0.5–1.

The peak position (near 1600 cm^{-1}) of the G band in the spectra of C:H nanofilms, its relatively small width, and the presence of the D band of comparable intensity indicate that sp^2-hybridised carbon atoms in these films enter the composition of polycyclic aromatic hydrocarbon (PAH) clusters [35–37]. The number of hexagonal rings composed of carbon atoms in these clusters ($N \approx 9$) can be estimated based on the results of [6,30,31,35–37], proceeding from the value E_{04} = 2.7 eV. These crystallites are ~1 nm in size [6,36,37]. The crystallite parameters barely change after applying one cleaning pulse. It

should be noted that PAH-based C:H films are intensively studied, being considered as promising antifriction coatings [6, 35–37].

Note another important fact. All processes of C:H nanofilm synthesis and annealing by laser radiation were performed in air. Despite this fact, no traces of (at least) nitrogen were observed in the Raman spectra of these films. Therefore, air is not a hindrance for the synthesis of C:H nanofilms on the surface of optical materials via annealing oil by high-power KrF EBL radiation, provided that the irradiated surface area is ~1 cm^2.

4. Laser-induced damage of quartz samples

As was noted above, the transition from the cell-based scheme described in [8, 9] to the scheme with a TO layer deposited on the output surface of quartz substrates was a forced measure, because cell windows 13 mm in diameter damaged at LR fluences about 2 J cm^{-2} and a laser spot size of 1 cm. Larger substrates from the second set were damaged as well if they were mechanically strained as a result of rigid fastening. Since it was necessary to reduce the internal stress in substrates to minimum, they were basically exposed to laser radiation as free-standing samples.

In this version, the laser damage threshold for quartz substrates decreased with an increase in the absorption coefficient of the layer on the substrate output surface and an increase in the surface layer density (product of the layer material density by the layer thickness). For example, for the quartz plates from the first set, coated by a black carbon layer ~1 μm thick and $\alpha(250\ \text{nm}) \approx 2 \times 10^5$ cm^{-1} (which was obtained by vacuum annealing of a polymerised film of furfuryl alcohol), the damage near the sample input surface was very strong even at $F = 2.9$ J cm^{-2}, as can be seen for sample 12 in Fig. 7.

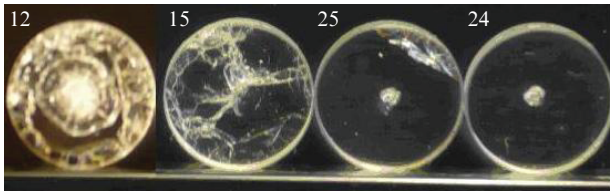

Figure 7. Photographs of the input surfaces of damaged samples 12, 15, 25, and 24 from the first set.

Silicone oil was applied instead of TO in some experiments. This oil is denser, harder, and more viscous. Generally, its layer was much thicker (~100 μm) than TO layers. One of plates coated with this layer withstood one pulse with $F = 3.6$ J cm^{-2}, but a network of cleavages was formed near its input surface after the second pulse with $F = 3.3$ J cm^{-2} (Fig. 7, sample 15). A decrease in the thickness of silicone oil layer to ~10 μm increased the breakdown threshold to about 4 J cm^{-2}.

The damage threshold for quartz plates from the first set with a TO layer ~10 μm thick was ~5.7 J cm^{-2}. Sample 24 with a TO layer (Fig. 7) withstood a pulse with $F = 6.8$ J cm^{-2}. There is a cleavage on the input surface of this sample within a spot about 1 mm in size. Sample 25 was exposed to two pulses, acting on newly deposited oil layers. After the first pulse with $F = 5.8$ J cm^{-2}, no visual damage was observed for this sample. Damage appeared after the second pulse with $F = 5.2$ J cm^{-2}. In addition to the cleavage at the centre of the input surface, cleavages were also formed in the lower part, where oil saggings were present on the opposite surface (they are on the top for sample 25 in Fig. 7). Quartz samples 13 mm in diameter from the first set were not damaged in the following TO annealing regime: first an oil film was exposed to one pulse with $F = 5.7$ J cm^{-2}, and then it was processed by four cleaning pulses with F decreasing from 5.7 to 5 J cm^{-2}. The maximum intensity I_L reached 70 MW cm^{-2} in this case.

The laser breakdown threshold for larger quartz samples from the second set (20 mm in diameter and 6 mm thick) was higher: they withstood irradiation of an oil film by one pulse with $F = 6$ J cm^{-2} and exposure to four cleaning pulses with fluences ranging from 5.7 to 5.5 J cm^{-2}. Experiments with a KU-1 glass plate 100 mm in diameter and 10 mm thick showed that it withstands different regimes of annealing of absorbing films on the output surface at LR fluences up to 8 J cm^{-2}.

The spatial separation of the areas of LR absorption (quartz substrate output surface) and the damaged regions (near the input surface) indicates that the damage is caused by shock waves, and the pressure jump in these regions near the breakdown is close to the breaking strength of quartz glass, i.e., to ~10^8 Pa [38].

This pressure jump arises when a layer of oil (or some other material that strongly absorbs LR) on the glass plate output surface is transformed into plasma. According to the estimates [39], the laser plasma temperature is close to ~1 eV at $I_L \approx 10$–100 MW cm^{-2}. Specifically the transformation of TO into plasma on the glass surface during ~10 ns induces a shock wave in the glass with a pressure jump up to 10^7–10^8 Pa. Similar pressure jumps in shock waves (although under somewhat different experimental conditions) were observed in [40]. Shock and sound waves with frequencies ~10^8 Hz rapidly decay in quartz glass: by a factor of about two on a length of 1 cm [38]. This circumstance may explain the experimentally observed increase in the laser damage threshold for large KU-1 glass plates.

The appearance of damage in the experiments with quartz samples from the first set was rather unusual: at a small excess above the LR damage threshold, there were cleavages about 1 mm in diameter and depth at the centre of the input substrate surface, as for samples 24 and 25 in Fig. 7. Why such small cleavages are formed at the substrate centre, while the irradiated spot area is 1 cm in diameter and an almost plane shock wave of the same transverse size is formed? This question was answered based on the results of [41]. Let us cite three statements from this study, which are of key importance for the case under consideration:

(i) "deformation bands never arise in samples under conditions of one-dimensional (uniaxial) loading by a plane shock wave";

(ii) "localised-deformation bands under pulsed loads are due to the interference of unloading waves; the negative stress does not exceeds the material strength within this interference zone"; and

(iii) "unloading wave sources are free surfaces".

A complex consideration of these statements in the analysis of the reasons for the occurrence of 'point' cleavages at the centre of the glass sample input surface shows that these cleavages are due to the axial symmetry of both the samples and the LR spot. In this case, along with a plane shock wave moving between the flat faces of the sample, there is also a wave reflected from its lateral cylindrical surface, which is focused into the sample centre. As a result, the sum of the

shock waves reaches a maximum intensity at the centre of the input sample surface. The general structure of the intensity distribution for interfering shock waves over the entire sample corresponds to the structure of the damage near the input surface of sample 12, which is observed at a relatively large excess above the 'point' damage threshold.

The above-cited statements from [41] also gain insight into the form of quartz sample damage in the presence of oil saggings: the latter locally increase the intensity and duration of the forward shock waves and the waves reflected from the lateral face. The role of internal mechanical stress, which significantly reduces the shock strength of the samples, is also clarified.

The aforementioned factors must be taken into account when planning experiments on carbon nanofilm synthesis by annealing TO films on quartz glass substrates using KrF laser radiation. To increase the laser damage thresholds for substrates and, therefore, the ultimate thicknesses of nanofilms synthesised on them, it is desirable to use mechanically unstrained samples with transverse sizes significantly exceeding the laser spot diameter and flat lateral faces, which cannot focus reflected shock waves.

Along with quartz glass, other optical materials transparent for UV LR can be used in the above-described experiments. In particular, we tested high-purity fluorite plates; the radiative strength of this material was studied previously in [33]. The output surface of the CaF_2 samples with TO films was covered by fine-structure cracks even after one LR pulse with $F = 3$ J cm^{-2}. The cracking of the surface contacting laser plasma is due to not only the lower (in comparison with quartz glass) mechanical strength of CaF_2 but also to the larger (by a factor of 30 as compared with KU-1) LR absorption coefficient at $\lambda = 248$ nm, induced by ionising radiation (short-wavelength radiation from plasma) [24, 25]. The latter factor causes overheating of a thin substrate surface layer with its subsequent cracking.

Strong induced absorption is also typical of MgF_2 crystals [24]. Therefore, one would expect laser damage of the same type for this material during oil layer annealing by KrF laser radiation as for CaF_2.

Induced LR absorption at $\lambda = 248$ nm is practically absent in sapphire [24]. This circumstance, along with the high strength characteristics of this material, makes sapphire substrates promising for nanofilm synthesis using high-power KrF EBL radiation (according to the above-described scheme of oil layer annealing in air). First test experiments with sapphire samples proved these expectations.

5. Conclusions

The main result of our study is that we proved the possibility of synthesising C:H nanofilms with an area of ~1 cm^2 on KU-1 glass substrates as a result of annealing a thin oil layer on the glass surface in air by high-power KrF laser radiation applied to the glass–oil interface through the glass. After the exposure of a thin TO layer to one or two 80-ns LR pulses with a fluence of ~5 J cm^{-2}, a C:H film up to 40 nm thick remains on the glass surface. An analysis of these films by optical and Raman spectroscopy showed that they contain ~40 at% hydrogen, have an optical gap $E_{04} \approx 3$ eV, and consist of PAH clusters ~1 nm in size with a number of graphite rings up to 10. Using exposure to cleaning laser pulses (also in air), one can change the characteristics of nanofilms, transforming them from polymer- to graphite-like ones.

The laser synthesis of C:H nanofilms in air, which was proposed and implemented for the first time, makes it possible to exclude currently used vacuum technologies (at least when depositing films on quartz or sapphire substrates). In principle, nanofilms can be synthesised using radiation of high-power lasers with other wavelengths, as well as layers of other oil liquids, due to which the ranges of both the OMs serving as substrates and the film compositions can be expanded.

The ultimate fluence $F \approx 6$ J cm^{-2} for oil layer annealing by KrF laser radiation was determined by the occurrence of quartz substrate damage. This damage was caused by shock waves with a pressure jump up to 10^8 Pa, induced by the laser plasma formed on the substrate surface at LR intensities up to 100 MW cm^{-2}. The most important factor determining the damage threshold for substrates is their geometric shape, which sets the intensity pattern for the sum of shock waves reflected from all surfaces. Cylindrical lateral surfaces of substrate, which focus reflected shock waves into its centre, are most hazardous in this context. These results allowed us to reveal some new nuances, which must be taken into account when analysing the laser-induced damage of OM products. They are expected to be useful for experts in laser physics and technology.

Acknowledgements. We are grateful to V.I. Kozlovskii and K.Kh. Pilosyan for their great help in spectral measurements.

References

1. Spitsyn B.V., Aleksenko A.E. *Zashch. Met.*, **43** (5), 456 (2007).
2. Konov V.I. *Laser Photonics Rev.*, **6** (6), 739 (2012).
3. Salvatori S. et al. *Laser Phys.*, **26**, 064005 (2016).
4. Belenkov E.A., Greshnyakov V.A. *Fiz. Tverd. Tela*, **58**, 2069 (2016).
5. Konshina E.A. *Amorfnyi gidrogenizirovannyi uglerod i ego primenenie v opticheskikh ustroistvakh* (Amorphous Hydrogenated Carbon and Its Applications in Optical Devices) (St. Petersburg: SPb NIU ITMO, 2010) p. 91.
6. Robertson J. *Mater. Sci. Eng. R*, **37**, 129 (2002).
7. Han Tae-Hee et al. *Mater. Sci. Eng. R*, **118**, 1 (2017).
8. Lyalin A.A. et al. *Quantum Electron.*, **29** (4), 355 (1999) [*Kvantovaya Elektron.*, **27**, 73 (1999)].
9. Simakin A.V., Lubnin E.N., Shafeev G.A. *Quantum Electron.*, **30**, 263 (2000) [*Kvantovaya Elektron.*, **30**, 263 (2000)].
10. Kompanets V.O. et al. *Laser Phys.*, **26**, 066002 (2016).
11. Ralph F.D. *SPIE Newsroom* (2012); https://doi.org/10.1117/2.120121.004030.
12. Borisov V.M., Demin A.I., Khristoforov O.B. *Quantum Electron.*, **45**, 200 (2015) [*Kvantovaya Elektron.*, **45**, 200 (2015)].
13. Sergeev P.B. *J. Sov. Laser Res.*, **14** (4), 237 (1993).
14. Obenschain S. et al. *Appl. Opt.*, **54** (31), F103 (2015).
15. Kantsyrev V.L. et al. *Pis'ma Zh. Tekh. Fiz.*, **17** (2), 56 (1991).
16. Kantsyrev V.L., Sergeev P.B., Tyunina M.A. *Pis'ma Zh. Tekh. Fiz.*, **17** (17), 29 (1991).
17. Kantsyrev V.L., Sergeev P.B., Tyunina M.A. *Pis'ma Zh. Tekh. Fiz.*, **18** (6), 63 (1992).
18. Kantsyrev V.L., Sergeev P.B., Tyunina M.A. *Pis'ma Zh. Tekh. Fiz.*, **18** (20), 32 (1992); **18** (20), 36 (1992).
19. Barabanov V.S. et al. *J. Sov. Laser Res.*, **14** (6), 421 (1993).
20. Sergeev P.B., Sergeev A.P. *Quantum Electron.*, **40**, 804 (2010) [*Kvantovaya Elektron.*, **40**, 804 (2010)].
21. Sergeev A.P., Sergeev P.B. *Kratk. Soobshch. Fiz. FIAN*, **41** (10), 11 (2014).
22. Sergeev P.B., et al. *Sbornik materialov VI Vserossiiskoi konferentsii po nanomaterialam (NANO 2016) (Proc. VI All-Russia Conference on Nanomaterials (NANO 2016))* (Moscow, 2016) p. 156; http://www.nano.imetran.ru.
23. Lipshtein R.A., Shakhnovich M.I. *Transformatornoe maslo* (Transformer Oil) (Moscow: Energoatomizdat, 1983) p. 296.
24. Barabanov V.S., Sergeev P.B. *Quantum Electron.*, **25**, 717 (1995) [*Kvantovaya Elektron.*, **22**, 745 (1995)].

25. Sergeev P.B., Sergeev A.P., Zvorykin V.D. *Opt. Zh.*, **76**, 13 (2009).
26. Theye M.-L., Paret V., Sadki A. *Diamond Relat. Mater.*, **10**, 182 (2001).
27. Konov V.I. et al. *Sov. J. Quantum Electron.*, **21**, 1112 (1991) [*Kvantovaya Elektron.*, **18**, 1226 (1991)].
28. Komlenok M.S. *Extended Abstract of Candidate's Dissertation* (Moscow, IOF RAN, 2008).
29. Ferrari A.C. *Diamond Relat. Mater.*, **11**, 1053 (2002).
30. Casiraghi C., Ferrari A.C., Robertson J. *Phys. Rev. B*, **72**, 085401 (2005).
31. Casiraghi C. et al. *Diamond Relat. Mater.*, **14**, 1098 (2005).
32. Awazu K., Kawazoe H. *J. Appl. Phys.*, **94**, 6243 (2003).
33. Sergeev P.B., Sergeev A.P., Zvorykin V.D. *Quantum Electron.*, **37**, 706 (2007) [*Kvantovaya Elektron.*, **37**, 706 (2007)].
34. Sergeev P.B., Sergeev A.P., Zvorykin V.D. *Quantum Electron.*, **37**, 711 (2007) [*Kvantovaya Elektron.*, **37**, 711 (2007)].
35. Castiglioni C. et al. *J. Chem. Phys.*, **114**, 963 (2001).
36. Miller J.H. et al. *Proc. Comb. Instit.*, **34**, 3669 (2013).
37. Herdman J.D. et al. *Carbon*, **49**, 5298 (2011).
38. Grigor'ev I.S., Meilikhov E.Z. (Eds) *Handbook of Physical Quantities* (Boca Raton: CRC Press, 1996; Moscow: Energoatomizdat, 1991).
39. Grasyuk A.Z. *Vzaimodeistvie izlucheniya s veshchestvom* (Interaction of Radiation with Matter) (Moscow: Izd-vo FIAN, 2004) p. 320.
40. Zvorykin V.D. et al. *Laser Part. Beams*, **26**, 461 (2008).
41. Belikova A.F., Buravova S.N., Petrov E.V. *Zh. Tekh. Fiz.*, **83** (8), 68 (2013).